A simple and mild chemical oxidation route to high-purity nano-graphene oxide

Martin Rosillo-Lopez, Christoph G. Salzmann*

Department of Chemistry, University College London, 20 Gordon Street, London WC1H 0AJ, United Kingdom

Abstract

Nano graphene-oxide (nGO) is used in a wide range of applications including cellular imaging, drug delivery, desalination and energy storage. Current preparation protocols are similar as for standard graphene oxide (GO) and typically rely on mixtures of sulfuric acid and potassium permanganate. We present a new route to nGO (~30 nm diameter) using a quite defective arc-discharge carbon source and only 9 M nitric acid as the oxidising agent. The preparation can be scaled up proportionately with current GO protocols with 50 mL of half-concentrated nitric acid able to process one gram of arc-discharge material. The workup is straight forward and involves neutralisation with sodium hydroxide which precipitates the sodium salt of nGO from solution. The only by-product of the new procedure is aqueous sodium nitrate which makes this protocol the cleanest route yet to nGO. The presence and quantities of functional groups in our nGO are determined and compared with standard GO. We anticipate that this new route to nGO will foster a range of new applications. The presence of highly reactive carboxylic anhydride groups on our nGO material in particular offers an excellent opportunity for purpose-specific chemical functionalization.

* Corresponding author. e-mail: c.salzmann@ucl.ac.uk (Christoph G. Salzmann), tel.: +44 20 7679 8864

1. Introduction

As a single sheet of sp^2 hybridised carbon, graphene has received much attention in recent years for its remarkable physical properties.[1-5] Chemical oxidation of graphene to graphene oxide (GO), a single sheet of mixed sp^2 and sp^3 hybridised carbon with multiple oxygen functionalities such as alcohols, epoxides and carboxylic acids, is achieved through strong oxidation conditions.[6-9] More recently, nano-graphene oxide (nGO) whose dimensions are 1-2 orders of magnitude smaller than conventional GO have been utilised for therapeutics,[10] cellular imaging and drug delivery,[11] desalination[12] and lithium ion batteries[13] making this novel material highly desirable. The synthesis of nGO also requires strong oxidising conditions similar to those of GO and typically involves using large amounts of permanganate in a concentrated sulfuric acid medium.[11, 14-17] In some cases, the pre-oxidation of the carbon source was even found to be necessary.[14] Moreover, the workup typically requires lengthy repeated centrifugation[11, 15] and/or sonication steps[17] to isolate the supernatant containing the nGO. Consequently, a simple procedure for the synthesis of nGO is highly desirable in order to reduce the time needed for its preparation, as well as a cleaner, safer and more environmentally friendly approach which does not require potassium permanganate.

The changes in the chemical structure of GO upon thermal annealing under vacuum or inert gas conditions has proven to be controversial.[18-22] This is in part due to the many different ways in which GO can be synthesized, but also because *in-situ* measurements of GO at high temperature and high vacuum can be challenging. Most *in-situ* thermal measurements of GO involve monitoring changes in the functional groups using X-ray photoelectron spectroscopy (XPS)[18, 19] or Fourier Transform Infrared spectroscopy (FT-IR)[21]. Although both techniques are powerful tools in functional group elucidation there are significant drawbacks to either approach. In the case of XPS, peak fitting can be subjective and a significant degree of chemical knowledge of the structure in question is a prerequisite. Similarly, disambiguation of functional groups in FT-IR is difficult, particularly in the fingerprint region where many contributions from different functional groups exist.[23]

Here we aim to develop a new simple route for preparing nGO which does not rely on potassium permanganate as the oxidising agent. The resulting material is compared and benchmarked against the traditional GO in terms of structure, functional groups and thermal annealing behaviour.

2. Experimental

2.1. Preparation of nGO

Arc-discharge (ADC) material consisting of single-wall carbon nanotubes (SWCNT) (diameter: 0.7- 1.2 nm, length: 10-50 μm), multi-wall carbon nanotubes (MWCNT) (diameter: 8-20 nm, length: 2-20 μm) and graphitic carbon was purchased from the Materials and Electrochemical Research (MER) Corporation (MRSW grade). 420 mg of this material was ultrasonicated in 21 mL of 1:1 distilled water/conc. nitric acid for 30 min and then refluxed in air for 20 h, generating brown NO_x fumes. The resulting dispersion was diluted three fold with distilled water and then filtered under vacuum through a 0.2 μm track-etched Whatman polycarbonate membrane. The black residue on the membrane was kept to one side and the brown-black filtrate was neutralized by carefully adding NaOH pellets. On neutralization, precipitation of Na-nGO occurred. The mixture was then filtered under vacuum in the same way as before and the resulting filtrate (containing $NaNO_3$) was discarded. The Na-nGO left on the membrane was re-dispersed in ~0.1 M nitric acid and dialyzed against distilled water *via* a regenerated cellulose dialysis membrane from Spectrum Laboratories, MWCO 3.5 kDa, flat width 45 mm. The dialysis was considered complete when the conductivity of the surrounding water was <5 μS cm^{-1}. The purified dispersion was then freeze dried to obtain 90 mg (21 % yield by mass) of brown-black nGO material. A schematic of the preparation procedure is shown in Fig. 1.
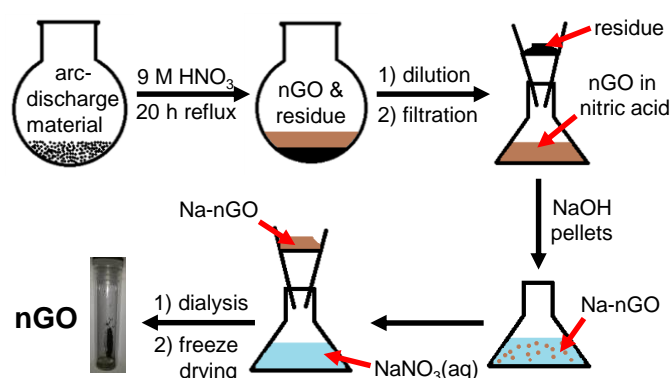
Fig. 1. Schematic illustration of the preparation of nGO.

2.2 Preparation of graphite oxide (GO)

For comparisons, GO was prepared following the modified Hummers method.[6] Graphite powder (1.00 g, <150 μm, Sigma Aldrich) was added to concentrated sulfuric acid (25 mL, 96% w/w) at 0°C with stirring. Potassium permanganate (3.00 g) was added slowly to the reaction mixture and the mixture was heated at 40°C for 30 minutes. Distilled water (50 mL)

was then added and the mixture stirred for a further 15 minutes at 95°C. The resulting brown mixture was then diluted by addition of distilled water (175 mL) followed by dropwise addition of hydrogen peroxide (10 ml, 30% v/v). The resulting yellow-green mixture was filtered through a 0.2 μm polycarbonate membrane, washed with HCl (150 mL, 10% v/v) and allowed to dry. The dry powder was re-dispersed in distilled water (200 mL) and dialyzed against water using a pretreated standard grade, regenerated cellulose dialysis membrane (Spectrum Laboratories, MWCO 3.5 kDa). The GO was then exfoliated *via* ultrasonication for 90 minutes, and the dispersion was then centrifuged at 3000 rpm for 40 minutes and decanted to isolate the exfoliated GO. The GO was ultrasonicated once more for 30 minutes and the dispersion was filtered through glass wool. The filtrate was collected and passed over a cation exchange resin (Amberlite IR120, Sigma-Aldrich), concentrated and finally freeze dried to give ~1 g of a brown powder.

2.3 Sample Characterizations

X-ray photoelectron spectroscopy (XPS) measurements were carried out on a Thermo Scientific K-Alpha XPS machine with a monochromated Al K_α source (E=1486.6 eV), using a double focusing 180-degree hemisphere analyzer of ~125 mm radius and detected with a 18 channel position sensitive detector. A dual-beam flood gun delivering electrons and argon ions was used to compensate charge accumulation on the measured surfaces. All carbon samples were pressed onto an indium substrate for analysis to ensure no background contribution from other carbon sources. Survey scans were recorded three times with a resolution of 1 eV and pass energy of 200 eV whilst the elemental regions were recorded 10 times with a resolution of 0.1 eV and pass energy of 50 eV. In both cases, a 400 μm spot size and 50 ms dwell time was used for each scan.

High-resolution ^{13}C solid-state NMR spectra were recorded on a Bruker Avance 300 spectrometer with a 7.05 T wide-bore magnet at ambient probe temperature. The spectra were recorded at 75.5 MHz with a Bruker 4 mm double-resonance magic-angle spinning (MAS) probe using high-power proton decoupling (HPDEC). The operating conditions were ^{13}C 90° pulse duration = 3.7 μs; recycle delay = 120 s with 2145 transients. The nGO was packed into zirconia rotors of 4 mm external diameter and spun at 12 kHz MAS frequency with a stability greater than ±3 Hz. Tetramethylsilane (TMS) was calibrated against an aqueous solution of 4,4-dimethyl-4-silapentane-1-sulfonic acid (DSS, 0 ppm) and glycine (176.46 ppm), and the ^{13}C chemical shifts are reported with respect to TMS.

Attenuated total reflectance infrared spectroscopy (ATR-IR) spectra were collected on a Bruker Tensor 27 FTIR spectrometer using the attenuated total reflectance infrared spectroscopy mode (ATR-IR) fitted with a room temperature DLaTGS detector at 4 cm^{-1} resolution and a diamond crystal as the internal reflection element. A background spectrum was taken before measuring each sample, and both the background as well as sample spectra were allowed to collect for 256 scans.

Raman measurements were carried out using a Renishaw Ramascope using a 633 nm laser with a 50-fold magnification objective. Each scan was run for 20 seconds and accumulated 4 times to give the final spectra.

For AFM imaging, one drop of ~0.1 mg/mL aqueous dispersion of the nGO was spin coated onto freshly cleaved 'highly oriented pyrolytic graphite' (HOPG) using a Laurell Technologies WS-650 spin-coater (5000 rpm). A digital instruments multimode 8 nanoscope scanning probe microscope with a Bruker nanoscope IV controller was used in the tapping mode with an 'E' scanner for recording AFM images.

For TEM imaging, one drop of ~0.1 mg/mL aqueous dispersion of the nGO was drop coated onto a lacy carbon TEM grid. The TEM measurements were then performed on a Jeol CX100 TEM with a tungsten filament and a Gatan Erlanshen ES500W camera.

For thermal analysis, 2.5 mg of nGO were heated inside a quartz-glass tube from room temperature to 900°C at a rate of 10°C min^{-1} under high vacuum conditions (~1.5 x 10^{-5} mbar base pressure) using a Carbolite MTF 1200 horizontal tube furnace. The *in-situ* mass spectrometry of the desorbing species was recorded every 5°C in the 1 to 200 *m/z* range using a HAL RC 201 mass spectrometer from Hiden Analytical with a Faraday Cup detector. Prior to ATR-IR measurements, individual nGO samples were heated from room temperature to a given temperature in this setup. Once a certain temperature had been attained the samples were allowed to cool down to room temperature before leaking to ambient pressure. The ATR-IR spectra were recorded immediately afterwards.

Optical absorbance spectra were recorded in quartz cuvettes (path length = 10 mm) on a PerkinElmer Lambda 365 UV/VIS spectrophotometer at steps of 1.0 nm and scan rate of 100 nm min^{-1}.

Thermogravimetric analysis (TGA) of the ADC (MER) material was performed in air at a heating rate of 3°C min^{-1} on a SETARAM SETSYS 16/18 instrument.

3. Results and Discussion

3.1 Characterization of nGO

The AFM image of nGO in Fig. 2(a) shows that the flakes are of nanoscale dimensions. The average lateral dimensions are 23 ± 5 nm for the shortest length and 31 ± 6 nm for the longest length, respectively (*cf.* Fig. 2(b)). The average height of the flakes is ~2.7 nm as shown in Fig. 2(c) which corresponds to ~3 oxidized carbon layers.[11, 14] However, some of the flakes can be seen to have 'dome-like' features suggesting that smaller flakes may have adsorbed onto the larger ones. The adsorption of smaller fragments onto larger nGO flakes has been previously observed for other nGO materials.[11] Considering the hydrophilic nature of nGO it seems possible that adsorbed water could also contribute to the measured heights.

A TEM image of nGO is shown in Fig. 2(d) where the nGO flake is indicated by a red arrow. It was found from several additional TEM images of nGO that the lateral dimensions were within error of the AFM measurements with the shortest and longest lengths determined to be 32 ± 10 nm and 43 ± 15 nm, respectively (*cf.* Figure 2(e)). The slightly larger dimensions in TEM compared to the AFM analysis is expected to be due to flakes overlapping with each other as a consequence of the drop-coating process.
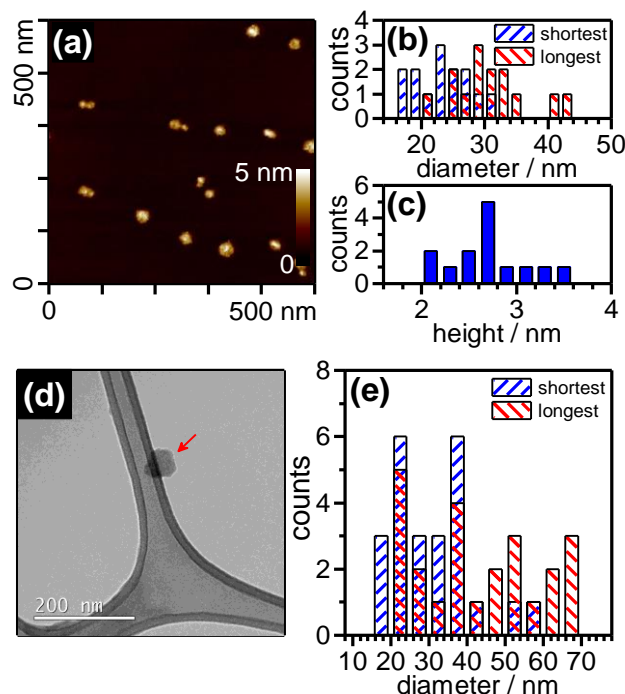
Fig. 2. (a) AFM image of nGO spin-coated onto an HOPG substrate, (b) AFM diameter distribution of nGO showing the shortest (blue) and longest (red) lateral lengths, (c) AFM height distribution of nGO, (d) TEM image of an nGO flake drop-coated onto a lacy carbon

grid and (e) diameter distribution of nGO from TEM analysis. Additional AFM and TEM images of nGO are shown in Figures S1 and S2 the Supplementary Information.

Raman spectra of our nGO, GO, the solid residue after the nitric acid oxidation as well as of the as-received ADC material from MER corporation are shown in Fig. 3. The presence of radial breathing modes (RBM) below 200 cm^{-1} and the splitting of the G band (~1590 cm^{-1}) into G$^+$ and G$^-$ components in the ADC spectrum confirm that the starting material is rich in carbon nanotubes.[24, 25] The broad and intense D band (~1306 cm^{-1}) in the ADC spectrum gives rise to an I_D/I_G peak intensity ratio of 0.46 ± 0.07 indicating a significant amount of structural defects.[24-27] A similar case can be made for the broad 2D peak (~2618 cm^{-1}) which is usually more intense for high-quality SWCNTs.[27] After oxidation of the ADC material, the RBM and 2D modes can still be seen in the Raman spectrum of the insoluble residue albeit at lower intensities. The G band splitting is no longer clearly seen, and the D band has grown more intense (I_D/I_G = 0.74 ± 0.02) and is shifted to higher wavenumbers (~1347 cm^{-1}). This suggests that the residue contains oxidized CNTs but also other oxidized and insoluble carbon species which are likely to coat the CNTs.[28] This is confirmed by the TEM analysis of the residue shown in Fig. S3. The nGO spectrum is similar compared to GO showing only G and D bands of comparable intensities. This could suggest that the sp^2 domains of nGO and GO have comparable dimensions.
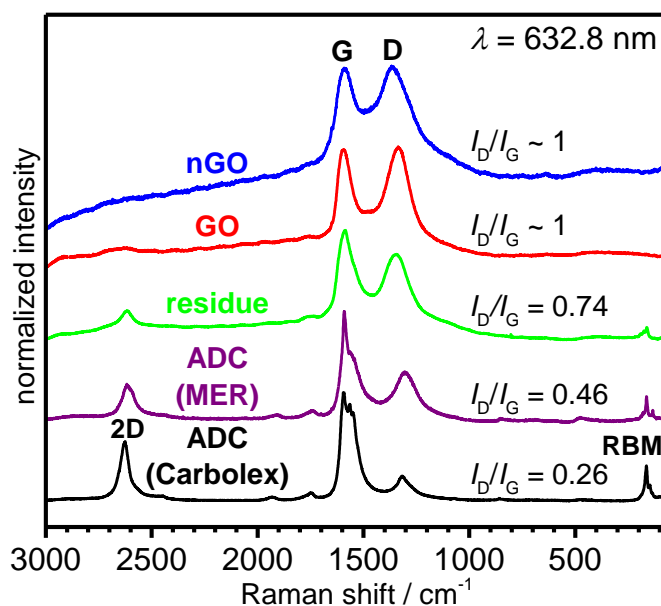
Fig. 3. Raman spectra of nGO (blue), GO (red), the insoluble residue (green), as-received MER ADC (purple) and ADC (Carbolex) used in previous work (black).[29]

In our previous work using ADC material from Carbolex it was demonstrated that carboxylated graphene nanoflakes containing very little or no basal plane oxygen functionality can be prepared using a similar oxidation procedure with 9 M nitric acid as reported here.[29] The formation of the more oxidized nGO using the ADC material from MER can be explained by considering the defectiveness of the ADC starting material. In the case of nGO, the I_D/I_G ratio of the starting ADC (MER) is considerably higher than that of the ADC (Carbolex) material ($I_D/I_G = 0.26 \pm 0.03$) which was used to prepare the carboxylated graphene flakes in ref. [29]. In other words, a certain degree of defectiveness seems to be required so that the graphene nanoflakes can be 'cut out' of graphenic carbon using 9 M nitric acid. Yet, a high degree of defectiveness means that the graphene nanoflakes are additionally oxidized to nGO. The fact that the residue material contains CNTs coated with debris strongly suggests that all carbon species present in the starting material take part in the reaction with 9 M nitric acid apart from the most defect-free CNTs (*cf.* Fig. S3).

Thermogravimetric analysis of the ADC (MER) material in Fig. S4 shows significant mass loss up to 325°C which is attributed to the burning of the amorphous carbon present in the ADC material. Treatment of the ADC (MER) material with 9 M nitric acid after heating to 325°C in air leads to a significantly less colored filtrate compared to the as-received material as shown in Fig. S5 (28% of the absorbance at 500 nm). This indicates that the amorphous carbon in the ADC material is a major source for the formation of nGO. In ref.

[29] we have shown that other carbon materials, such as graphite, carbon nanopowder and arc-discharge MWCNT, do not yield dispersible carbon materials after reaction with 9 M nitric acid.

The XPS survey spectrum of nGO shown in Fig. 4(a) illustrates the purity of the nGO material which contains only carbon and oxygen. Typical impurities of carbon nanomaterials such as nitrogen or ionic species are absent. The C/O atomic ratios of nGO, the residue after oxidation, GO and ADC (MER) decrease in the order ADC > residue > GO $\approx$ nGO in line with an increasing degree of oxidation (*cf.* Fig. 4(a)). Comparison of the C1s regions of GO and nGO in Fig 4(b) shows that the relative peak areas of the peaks centered at ~288.6 eV, which are attributed to C(III) species such as carboxylic acids, lactones and anhydrides,[30] are significantly larger for nGO compared to GO indicating a larger presence of C(III) species on the nGO. However, the peaks centered at ~286.9 eV, associated with C(I) species such as epoxides and alcohols, and C(II) species such as ketones[31, 32] are considerably less intense for the nGO indicating that fewer of these groups are present on nGO compared to GO. According to the Lerf-Klinowski model,[33] GO has both edge as well as basal-plane functionality with the former containing carboxylic acids, alcohols and to a lesser extent ketones, and the latter epoxides and alcohols. Hence, the carboxylic acid groups are largely localized at the edges of GO. The XPS spectrum of nGO is therefore strongly indicative of a significantly increased edge to basal plane ratio, as evidenced by the increased intensity of the C(III) region and the reduced intensity of the C(I)/C(II) region. This is consistent with the expectation of an nGO sheet having a higher edge to basal-plane ratio.
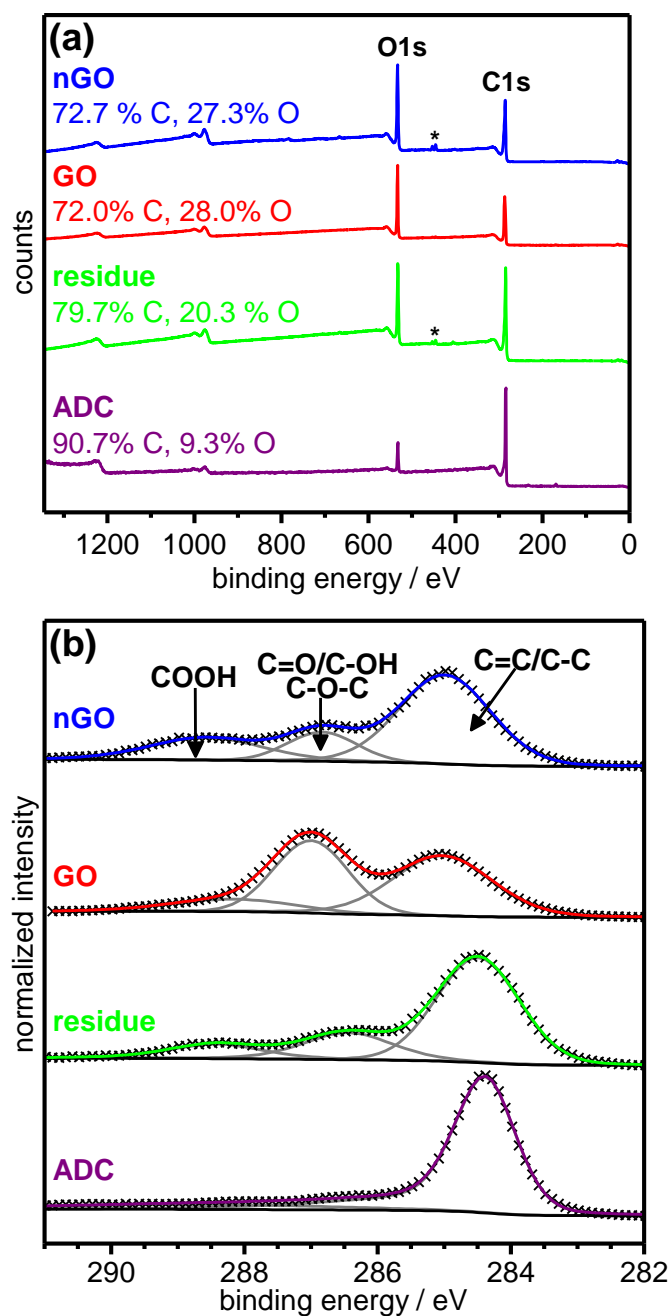
Fig. 4. (a) XPS survey spectra and (b) C1s regions of nGO (blue), GO (red), the residue (green) and the ADC material (purple). Peaks marked with asterisks in the survey spectra are due to the indium substrate. The C1s regions have been normalised with respect to the areas of the entire C1s features. The crosses in the C1s regions are the experimental data whereas the black, grey and coloured lines are the Shirley background functions, fitted peaks and peak sums, respectively.

The preparation of nGO by using ultrasonication of GO has been reported in ref. [34] and a detailed analysis of the C1s region has been reported. The relative areas of the peaks located at ~285.0, ~286.9 and ~288.6 eV of their nGO were 44.9, 45.5 and 9.7%.[34] The

corresponding values for our nGO material are 64.0, 15.2 and 20.8% which illustrates that our nGO material is more carboxylated but overall more graphenic compared to the nGO material from the ultrasonication-breakdown of GO.

As expected, the C1s region of the ADC starting material shows no significant degree of oxidized carbon. Interestingly, the C1s region of the residue shows a similar distribution of peaks compared with nGO albeit at an overall lower degree of oxidation. The lower binding energy of the C-C/C=C peak in the spectrum of the residue at 284.4 eV, which is about 0.6 eV lower with respect to nGO, also suggests that the extent of oxidation is lower than for nGO.

The very broad absorption band between 3600 cm^{-1} and 2500 cm^{-1} for nGO in the ATR-IR spectrum in Fig. 5 is assigned to the strongly hydrogen-bonded O-H stretching modes of carboxylic acids.[35] Furthermore, the peak at ~1720 cm^{-1} is characteristic for the C=O stretching mode of carboxylic acids.[36] Overall, the IR spectra of nGO and GO are remarkably similar. Yet, the peaks are generally broader for nGO suggesting a higher degree of variability in the local environments of the various functional groups. Given the many overlapping modes of functional groups below about 1500 cm^{-1} it is not possible to unambiguously correlate specific frequencies to a particular functional group. For instance, the broad band at ~1225 cm^{-1} is known to have contributions from ν_s(C-O) in both alcohols and carboxylic acids as well as the breathing mode (ring stretching) of the epoxide group.[21] In corroboration with XPS, the IR spectrum of the residue shows similar, although lower intensity features with respect to the spectrum of nGO, in compliance with the residue being less oxidized than nGO. As expected, the spectrum of ADC shows only weak features consistent with the low oxygen content of the starting material.
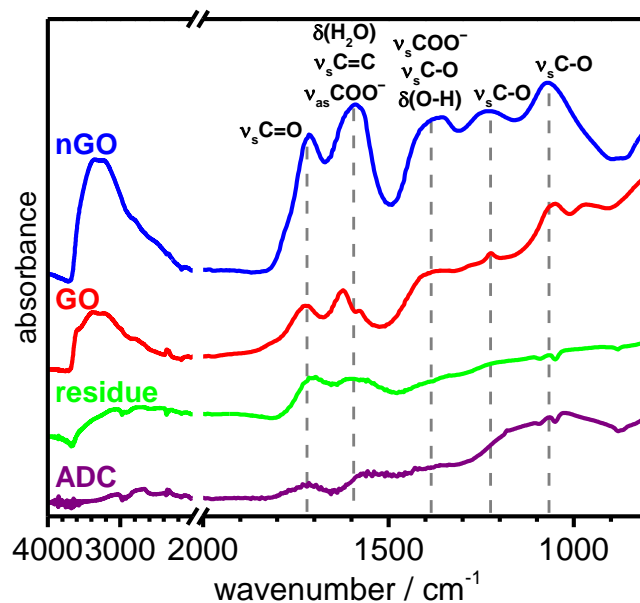
Fig. 5. ATR-IR spectra of nGO (blue), GO (red), the residue (green) and the ADC material (purple).

The ^{13}C ssNMR spectrum of nGO in Fig. 6 reveals the presence of four distinct peaks at 194, 170, 132 and 73 ppm. The first three of these peaks (illustrated by the dashed lines) can be attributed to ketones, carboxylic acids and non-oxidized sp^2 carbon, respectively.[33] This is in good agreement with the peak positions found in GO for these functional groups. The peak centered at 73 ppm in nGO is likely to be a combination of overlapping epoxide and alcohol groups, which are usually found at 70 ppm and 60 ppm (as shown by the dashed lines) respectively in GO. The ssNMR data is consistent with the XPS data in Fig. 4 showing larger amounts of C=O and COOH functional groups, and less hydroxyl and epoxide groups for nGO compared to GO. The slight down-fielding effect seen in the overlapping hydroxyl/epoxide peak in nGO at 73 ppm can be explained by the small flake size of nGO where hydroxyl groups situated at the edge are in close proximity to electron withdrawing carboxylic acid groups. Thus, the deshielding of these hydroxyl carbons results in a slight increase in chemical shift.
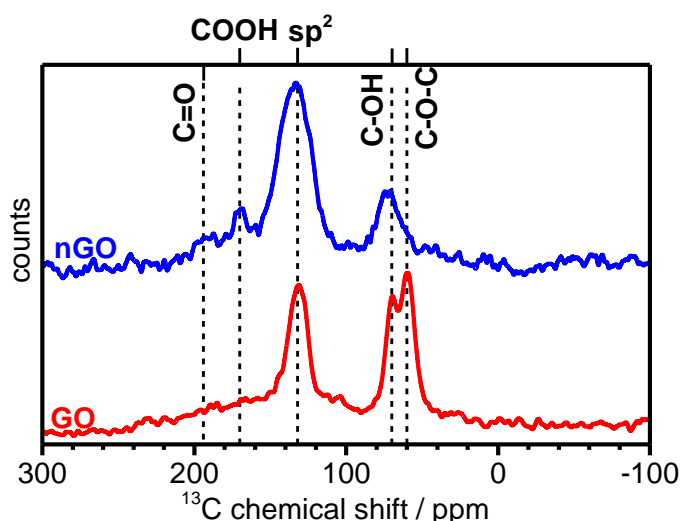
Fig. 6. ^{13}C ssNMR spectra of nGO (blue) and GO (red). Vertical dashed lines denote peak positions of functional groups as seen for GO.

On the basis of all structural characterizations, the structure of our nGO can be envisaged to be similar to the structure depicted in Fig. 7 which is analogous to a GO sheet of nanoscale dimension.
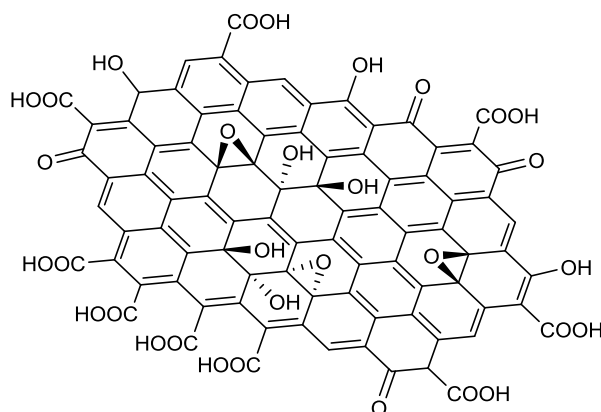
Fig. 7. Chemical structure of a very small nGO flake. The actual lateral dimensions are ~30 nm as shown in Fig. 2.

3.2 Heating of nGO under high vacuum conditions

The *in-situ* mass spectrometry data of nGO heated to 900°C in a high-vacuum is shown in Fig. 8(a). Below 250°C, the desorption of a gaseous species at $m/z = 18$ is observed which is attributed to H_2O. In our previous work with highly carboxylated graphene nanoflakes (cx-GNFs),[37] we have shown that H_2O desorption is primarily due to physisorbed water but also involves a contribution from water loss due to cyclic carboxylic anhydride formation at $T > 200$°C as the result of an intramolecular 'attack' between adjacent carboxylic acid groups.

13

This is also seen in our nGO, although to a lesser extent, from the ATR-IR spectra in Fig. 8(b) which show the gradual emergence of two new peaks at 1776 cm^{-1} and 1836 cm^{-1} after heating above 200°C. These are assigned to the asymmetric and symmetric anhydride stretching modes.[38] The anhydride groups were previously found to be more thermally stable with respect to carboxylic acid groups and consequently underwent decarboxylation at a later stage than carboxyl groups.[37] A similar trend is seen for the nGO which shows a sharp CO_2 loss at $m/z = 44$ centered at ~290°C with a long 'tail' up to 480°C indicating the initial decarboxylation of the carboxyl groups and later the decomposition of the anhydride groups. After decarboxylation of the anhydride groups the resulting C=O species decarbonylate giving rise to CO loss above 350°C. The amount of CO_2 released in nGO is much lower compared with the cx-GNFs which is in good agreement with nGO containing fewer COOH groups. However, the fact that nGO can form cyclic anhydrides provides strong evidence for presence of COOH groups in significantly large quantities at the graphene edge consistent with the earlier XPS and ssNMR data. It is noted that hydroxyl groups, which may also be present at the graphene edge, could in principle react with carboxylic acids to form lactones. However, these are discounted on the basis that the C=O stretching modes of lactones are typically found at lower frequencies than anhydrides (*i.e.* < 1800 cm^{-1}).[39]
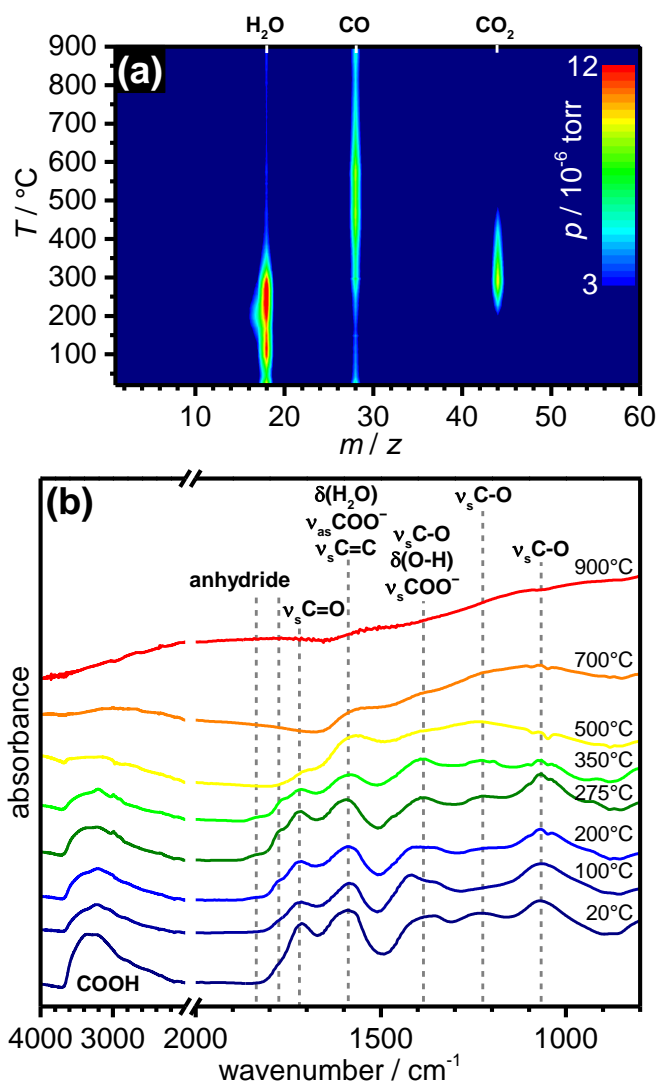
Fig. 8. Thermal annealing of nGO under high-vacuum conditions. (a) *In situ* mass spectrometry patterns and (b) ATR-IR spectra recorded at room temperature after heating to the indicated temperatures.

Above 480°C, no more CO_2 release is observed and therefore all decarboxylation processes have taken place. This is in good agreement with the IR spectrum recorded after heating to 500°C (*cf.* Fig. 8(b)) which shows a significant loss of O-H stretching between 3600 cm^{-1} and 2500 cm^{-1}, as well as the complete disappearance of the anhydride peaks. Interestingly, the retention of a weak but significant peak at ~1720 cm^{-1}, which later disappears after heating to 700°C, suggests that this carbonyl stretching mode is associated with a functional group which cannot undergo decarboxylation such as ketones. Mass spectrometry consistently shows a loss of CO only between 500 and 700°C which therefore strongly suggests that the functional groups indicated by the 1720 cm^{-1} peak are ketones and/or aldehydes. This is in good agreement with the ssNMR data of nGO which shows a higher concentration of ketones

than is commonly found for GO (*cf.* Fig. 6). The idea of carboxylic acids being less thermally stable than ketones in GO has also been reported by Ganguly *et al*. using *in-situ* XPS.[19]

The most intriguing peak in the IR spectrum of thermally annealed nGO is the broad peak centered at ~1587 cm^{-1}, which has been the source of some controversy in the GO literature.[23, 40-43] This peak has commonly been assigned to C=C stretching modes as well as the asymmetric stretching mode of carboxylate.[23] However, a deuteration experiment of GO has revealed this peak to shift by ~$2^{1/2}$ wavenumbers to lower frequency which unambiguously means that this peak is associated with the bending mode of water.[23] This is understandable for GO which has a relatively low concentration of carboxyl groups and the C=C bonds present are not particularly IR active. Interestingly, heating nGO to 700°C shows that this peak is still present. One can therefore conclude that in case of nGO this peak should mainly be attributed to C=C stretching since water has been removed and COOH groups have decarboxylated at this temperature. This is also consistent with the ssNMR of nGO which has a larger contribution from sp^2 carbon than GO.

Discussion of the desorption of hydroxyls and epoxides from nGO is difficult mainly because it is unclear as to whether these species will desorb as H_2O, as CO or as an entirely separate species. Given the large amounts of H_2O and CO detected by mass spectrometry it is likely that a combination of reaction pathways between epoxides, alcohols and other functionality has led to these detected species. Overall, it is interesting to note that the thermal desorption pattern of gases from nGO is very different compared to standard GO for which a concerted evolution of H_2O, CO and CO_2 has been observed at ~250°C (*cf.* Fig. S7 in ref. 37 and refs [44-48]). In a reaction mechanism proposed by Acik *et al*.[21] H_2O initiates a radical chain reaction which propagates using the existing oxygen functionality present on GO. This in turn generates various oxygen containing radicals the nature and composition of which are dependent on the initial ratio of the native oxygen containing functional groups present on the GO. Hence, the desorption patterns of GO and consequently nGO will vary according to this ratio. However, some inference from the IR spectra of nGO can be achieved at $T \geq 700$°C since C=O groups from ketones and carboxylic acids are no longer present. The IR data shows the merging of the three broad peaks at ~1067 cm^{-1}, ~1225 cm^{-1} and ~1385cm^{-1} into one very broad feature. Assignment of these three peaks could be attributed to C-O stretching modes suggesting that many C-O environments now exist on the nGO which are then mostly removed on heating to 900°C. This is consistent with the CO desorption 'tail' in the mass spectrometry patterns between 700°C and 900°C. Hence, the data suggests that C-O species are hardest to be removed. This view is consistent with Ganguly *et al.* who showed

that phenolic groups are the last groups to be removed from GO upon thermal annealing. Furthermore, Acik *et al*. have also shown by *in-situ* FTIR spectroscopy that cyclic ethers on the edges of graphene are present on GO after thermal annealing to 850°C.

4. Conclusion

A simple and mild route to nGO using relatively defective ADC material and 9 M nitric acid as the oxidizing agent has been reported. Compared to previous procedures for making nGO[11, 14-17] we completely avoid using permanganate and concentrated sulfuric acid. Furthermore, our new procedure does not require the repetitive centrifugation and ultrasonication steps that are commonly employed in the synthesis of other nGOs,[11, 15, 17] and the only by-products are aqueous sodium nitrate and any unreacted carbon. The thermal annealing of nGO under high vacuum was also investigated and it was found that carboxylic anhydride formation is an important mechanism during the thermal annealing of nGO. Overall, we expect that our new route to nGO will lead to more wide-spread applications using the nGO carbon nanomaterial. Carboxylic acid anhydrides are highly reactive chemical species. The formation of these species on our nGO material therefore offers an exciting possibility for subsequent chemical functionalization with purpose-specific nucleophiles.

Acknowledgement

References

[1] Lee C, Wei X, Kysar JW, Hone J. Measurement of the elastic properties and intrinsic strength of monolayer graphene. Science. 2008;321:385-8.

[2] Loh KP, Bao Q, Eda G, Chhowalla M. Graphene oxide as a chemically tunable platform for optical applications. Nat Chem. 2010;2:1015-24.

[3] Bunch JS, Verbridge SS, Alden JS, van der Zande AM, Parpia JM, Craighead HG, et al. Impermeable atomic membranes from graphene sheets. Nano Lett. 2008;8:2458-62.

[4] Meric I, Han MY, Young AF, Ozyilmaz B, Kim P, Shepard KL. Current saturation in zero-bandgap, topgated graphene field-effect transistors. Nat Nanotechnol. 2008;3:654-9.

[5] Balandin AA, Ghosh S, Bao W, Calizo I, Teweldebrhan D, Miao F, et al. Superior thermal conductivity of single-layer graphene. Nano Lett. 2008;8:902-7.

[6] Chen J, Yao BW, Li C, Shi GQ. An improved Hummers method for eco-friendly synthesis of graphene oxide. Carbon. 2013;64:225-9.

[7] Hummers WS, Offeman RE. PREPARATION OF GRAPHITIC OXIDE. J Am Chem Soc. 1958;80:1339-.

[8] Marcano DC, Kosynkin DV, Berlin JM, Sinitskii A, Sun Z, Slesarev A, et al. Improved Synthesis of Graphene Oxide. ACS Nano. 2010;4:4806-14.

[9] Dimiev A, Kosynkin DV, Alemany LB, Chaguine P, Tour JM. Pristine Graphite Oxide. J Am Chem Soc. 2012;134:2815-22.

[10] Tian B, Wang C, Zhang S, Feng L, Liu Z. Photothermally Enhanced Photodynamic Therapy Delivered by Nano-Graphene Oxide. ACS Nano. 2011;5:7000-9.

[11] Sun XM, Liu Z, Welsher K, Robinson JT, Goodwin A, Zaric S, et al. Nano-Graphene Oxide for Cellular Imaging and Drug Delivery. Nano Res. 2008;1:203-12.

[12] Gahlot S, Sharma PP, Gupta H, Kulshrestha V, Jha PK. Preparation of graphene oxide nano-composite ion-exchange membranes for desalination application. RSC Adv. 2014;4:24662-70.

[13] Xu Y-T, Guo Y, Li C, Zhou X-Y, Tucker MC, Fu X-Z, et al. Graphene oxide nano-sheets wrapped Cu2O microspheres as improved performance anode materials for lithium ion batteries. Nano Energy. 2015;11:38-47.

[14] Luo J, Cote LJ, Tung VC, Tan ATL, Goins PE, Wu J, et al. Graphene Oxide Nanocolloids. J Am Chem Soc. 2010;132:17667-9.

[15] Liu Z, Robinson JT, Sun X, Dai H. PEGylated nanographene oxide for delivery of water-insoluble cancer drugs. J Am Chem Soc. 2008;130:10876-7.

[16] Imani R, Emami SH, Faghihi S. Nano-graphene oxide carboxylation for efficient bioconjugation applications: a quantitative optimization approach. J Nanopart Res. 2015;17:88.

[17] Rahmanian N, Hamishehkar H, Dolatabadi JEN, Arsalani N. Nano graphene oxide: A novel carrier for oral delivery of flavonoids. Colloids Surf B. 2014;123:331-8.

[18] Yang D, Velamakanni A, Bozoklu G, Park S, Stoller M, Piner RD, et al. Chemical analysis of graphene oxide films after heat and chemical treatments by X-ray photoelectron and Micro-Raman spectroscopy. Carbon. 2009;47:145-52.

[19] Ganguly A, Sharma S, Papakonstantinou P, Hamilton J. Probing the Thermal Deoxygenation of Graphene Oxide Using High-Resolution In Situ X-ray-Based Spectroscopies. J Phys Chem C. 2011;115:17009-19.

[20] Yamada Y, Yasuda H, Murota K, Nakamura M, Sodesawa T, Sato S. Analysis of heat-treated graphite oxide by X-ray photoelectron spectroscopy. J Mater Sci. 2013;48:8171-98.

[21] Acik M, Lee G, Mattevi C, Pirkle A, Wallace RM, Chhowalla M, et al. The Role of Oxygen during Thermal Reduction of Graphene Oxide Studied by Infrared Absorption Spectroscopy. J Phys Chem C. 2011;115:19761-81.

[22] Bagri A, Mattevi C, Acik M, Chabal YJ, Chhowalla M, Shenoy VB. Structural evolution during the reduction of chemically derived graphene oxide. Nat Chem. 2010;2:581-7.

[23] Dimiev AM, Alemany LB, Tour JM. Graphene Oxide. Origin of Acidity, Its Instability in Water, and a New Dynamic Structural Model. ACS Nano. 2013;7:576-88.

[24] Jorio A, Souza AG, Dresselhaus G, Dresselhaus MS, Swan AK, Unlu MS, et al. G-band resonant Raman study of 62 isolated single-wall carbon nanotubes. Phys Rev B. 2002;65:155412.

[25] Dresselhaus MS, Dresselhaus G, Jorio A, Souza AG, Saito R. Raman spectroscopy on isolated single wall carbon nanotubes. Carbon. 2002;40:2043-61.

[26] Ferrari AC, Robertson J. Interpretation of Raman spectra of disordered and amorphous carbon. Phys Rev B. 2000;61:14095-107.

[27] Puech P, Flahaut E, Bassil A, Juffmann T, Beuneu F, Bacsa WS. Raman bands of double-wall carbon nanotubes: comparison with single- and triple-wall carbon nanotubes, and influence of annealing and electron irradiation. J Raman Spectrosc. 2007;38:714-20.

[28] Salzmann CG, Llewellyn SA, Tobias G, Ward MAH, Huh Y, Green MLH. The role of carboxylated carbonaceous fragments in the functionalization and spectroscopy of a single-walled carbon-nanotube material. Adv Mater. 2007;19:883-7.

[29] Salzmann CG, Nicolosi V, Green MLH. Edge-carboxylated graphene nanoflakes from nitric acid oxidised arc-discharge material. J Mat Chem. 2010;20:314-9.

[30] Kundu S, Wang Y, Xia W, Muhler M. Thermal Stability and Reducibility of Oxygen-Containing Functional Groups on Multiwalled Carbon Nanotube Surfaces: A Quantitative High-Resolution XPS and TPD/TPR Study. J Phys Chem C. 2008;112:16869-78.

[31] Chiang TC, Seitz F. Photoemission spectroscopy in solids. Ann Phys (Leipzig). 2001;10:61-74.

[32] Yumitori S. Correlation of C-1s chemical state intensities with the O-1s intensity in the XPS analysis of anodically oxidized glass-like carbon samples. J Mater Sci. 2000;35:139-46.

[33] Lerf A, He HY, Forster M, Klinowski J. Structure of graphite oxide revisited. J Phys Chem B. 1998;102:4477-82.

[34] Goncalves G, Vila M, Bdikin I, de Andres A, Emami N, Ferreira RAS, et al. Breakdown into nanoscale of graphene oxide: Confined hot spot atomic reduction and fragmentation. Sci Rep. 2014;4:6735.

[35] Hadzi D, Novak A. INFRA-RED SPECTRA OF GRAPHITIC OXIDE. Trans Faraday Soc. 1955;51:1614-20.

[36] Brooks CJ, Eglinton G, Morman JF. INFRARED SPECTRA OF ARYL CARBOXYLIC ACIDS AND THEIR ESTERS. J Chem Soc. 1961:106-16.

[37] Rosillo-Lopez M, Lee TJ, Bella M, Hart M, Salzmann CG. Formation and chemistry of carboxylic anhydrides at the graphene edge. RSC Adv. 2015;5:104198-202.

[38] Yang CQ, Wang XL. Formation of cyclic anhydride intermediates and esterification of cotton cellulose by multifunctional carboxylic acids: An infrared spectroscopy study. Text Res J. 1996;66:595-603.

[39] Jones RN, Angell CL, Ito T, Smith RJD. THE CARBONYL STRETCHING BANDS IN THE INFRARED SPECTRA OF UNSATURATED LACTONES. Can J Chem. 1959;37:2007-22.

[40] Mermoux M, Chabre Y, Rousseau A. FTIR AND C-13 NMR-STUDY OF GRAPHITE OXIDE. Carbon. 1991;29:469-74.

[41] Szabo T, Berkesi O, Forgo P, Josepovits K, Sanakis Y, Petridis D, et al. Evolution of surface functional groups in a series of progressively oxidized graphite oxides. Chem Mater. 2006;18:2740-9.

[42] Kovtyukhova NI, Ollivier PJ, Martin BR, Mallouk TE, Chizhik SA, Buzaneva EV, et al. Layer-by-layer assembly of ultrathin composite films from micron-sized graphite oxide sheets and polycations. Chem Mater. 1999;11:771-8.

[43] Boehm HP, Heck W, Sappok R, Diehl E. SURFACE OXIDES OF CARBON. Angew Chem Int Ed. 1964;3:669-77.

[44] Qiu Y, Guo F, Hurt R, Külaots I. Explosive thermal reduction of graphene oxide-based materials: Mechanism and safety implications. Carbon. 2014;72:215-23.

[45] Meihua J, Hae-Kyung J, Tae-Hyung K, Kang Pyo S, Yan C, Woo Jong Y, et al. Synthesis and systematic characterization of functionalized graphene sheets generated by thermal exfoliation at low temperature. J Phys D: Appl Phys. 2010;43:275402.

[46] Kim F, Luo J, Cruz-Silva R, Cote LJ, Sohn K, Huang J. Self-Propagating Domino-like Reactions in Oxidized Graphite. Adv Funct Mater. 2010;20:2867-73.

[47] Shen B, Lu D, Zhai W, Zheng W. Synthesis of graphene by low-temperature exfoliation and reduction of graphite oxide under ambient atmosphere. J Mat Chem C. 2013;1:50-3.

[48] McAllister MJ, Li J-L, Adamson DH, Schniepp HC, Abdala AA, Liu J, et al. Single Sheet Functionalized Graphene by Oxidation and Thermal Expansion of Graphite. Chem Mater. 2007;19:4396-404.